Effect of hypoxia-HIF-1α-periostin axis in thyroid cancer

YE YANG[1*], JUNYI WU[2*], HUIQIN ZHU[3*], XIAOQIN SHI[4], JUN LIU[2], YANG LI[2] and MIN WANG[2]

Departments of [1]Obstetrics and Gynecology, and [2]General Surgery, Shanghai General Hospital,
Shanghai Jiao Tong University School of Medicine, Hongkou, Shanghai 200080; [3]Department of General Surgery,
Dongtai People's Hospital, Dongtai, Jiangsu 224200; [4]Department of Pathology, Shanghai General Hospital,
Shanghai Jiao Tong University School of Medicine, Hongkou, Shanghai 200080, P.R. China

Abstract. The incidence of thyroid carcinoma (TC) has exhibited a rapid increase in recent years. A proportion of TCs exhibit aggressive behavior. The present study aimed to investigate the potential role of hypoxia-hypoxia inducible factor 1 subunit α (HIF-1α)-periostin axis in the progression of TC. The upregulation of periostin and HIF-1α expression levels was detected in 95 clinical TC tissues as compared with normal thyroid tissues. Hypoxia promoted the viability and invasion of TC cells and this effect was inhibited by the downregulation of periostin. Hypoxia also induced the Warburg effect in TC and this effect was inhibited by the silencing of periostin. Further investigations revealed that hypoxia activated HIF-1α, which in turn regulated the expression of periostin. Immunoprecipitation and dual luciferase reporter assays demonstrated that HIF-1α upregulated the expression of periostin by binding to the promoter of periostin. On the whole, these findings suggest the existence of a hypoxia-HIF-1α-periostin axis in TC and indicate the role of this axis in the progression of TC.

Introduction

Thyroid cancer (TC) is the most commonly occurring malignant tumor of the endocrine system, and its incidence rate has exhibited an increasing trend in recent years (1-3). TC includes a variety of histological subtypes, of which papillary TC accounts for >90% of all thyroid tumors (4). Whereas the majority of TCs do not exhibit a highly aggressive behavior, a proportion of the TCs exhibit aggressive characteristics (5,6).

Correspondence to: Professor Min Wang, Department of General Surgery, Shanghai General Hospital, Shanghai Jiao Tong University School of Medicine, 85 Wujin Road, Hongkou, Shanghai 200080, P.R. China
E-mail: wangmin0501@hotmail.com

*Contributed equally

However, the molecular mechanisms promoting the development and aggressive transition of the disease remain poorly understood.

Periostin is an extracellular matrix protein that plays a crucial role in the progression of various malignancies (7,8). A previous study by the authors revealed that periostin was associated with the proliferation, invasion and metastasis of TC cells (9). However, the regulation of periostin in TC is not yet well understood.

Hypoxia is considered one of the hallmarks of the tumor microenvironment of malignant tumors, particularly during progression. Tumor cells transition from aerobic respiration to glycolysis as a mechanism to ensure the availability of energy for their survival, a phenomenon referred to as the Warburg effect (10,11). This unusual glucose metabolism pathway promotes glucose uptake and lactate production, which play a pivotal role in the occurrence and development of tumors. Hypoxia-inducible factor-1 (HIF-1) is known as the main regulator promoting the adaptation of tumors to hypoxia. HIF-1 is a transcriptional nuclear protein with a wide range of target genes that are associated with hypoxia adaptation, inflammatory development and tumor growth. HIF-1 contains two subunits, HIF1 subunit α (HIF-1α) of 120 kD and HIF-1 subunit β (HIF-1β) of 91-94 kD. HIF-1α is the active subunit and is regulated by hypoxia (12-14).

Using bioinformatics analysis methods, it was predicted that HIF-1α may be able to bind to the promoter of periostin and up-regulate periostin expression. Therefore, the present study aimed to explore whether hypoxia can promote the expression of periostin in TC, resulting in progression of the disease. In addition, the authors aimed to investigate the interaction between periostin and HIF-1α.

Materials and methods

Bioinformatics analysis. The promoter sequence of the target gene (periostin) was predicted using the NCBI database (https://www.ncbi.nlm.nih.gov/pubmed/). JASPAR is an open-access database of curated, non-redundant transcription factor (TF) binding profiles stored as position frequency matrices and TF flexible models for TFs across multiple species in six taxonomic groups (http://jaspar.genereg.net/). The possible binding of HIF-1α to the promoter of periostin was analyzed using JASPAR.

Patients and ethical statement. TC specimens were collected from 95 patients who underwent total thyroidectomy or lobectomy between January, 2020 and December, 2021 at the Shanghai General Hospital, Shanghai Jiaotong University School of Medicine (Shanghai, China) with a median age of 48 years (range, 21-78 years). The clinicopathological data of the patients are shown in Table SI) The present study was approved by the Ethics Committee for Clinical Research of Shanghai General Hospital, Shanghai Jiaotong University School of Medicine (approval no. 2019KY016). Written informed consent was obtained from all patients included in the study.

Cells and cell culture. Human TC cell lines (BCPAP and TPC-1) were obtained from the Shanghai Institute of Life Sciences, Chinese Academy of Sciences. The cells were maintained in Dulbecco's modified Eagle's medium (DMEM) containing 10% fetal bovine serum (FBS; MilliporeSigma) and placed in a humidified incubator at 37˚C and 5% CO_2. The TC cells in the hypoxic group were incubated in a modulator incubator with 94% N_2, 5% CO_2, and 1% O_2 to establish hypoxic conditions for 24 h. Cells in the normoxic group were cultured under normoxic conditions (atmosphere of 20% O_2). In the present study, BCPAP and TPC-1 cells expressed increased levels of paired box 8 and transcription termination factor 1 mRNA, as determined using RT-qPCR (data not shown), which are considered as the biomarker of differentiated TC cells (15).

Immunohistochemistry (IHC). Tissues were fixed overnight in 10% neutral formalin fixing solution at room temperature, and finally wax blocks were embedded with paraffin. The paraffin embedded tissue was cut into 4-μm-thick slices and then baked in an oven at 63˚C for 1 h. For periostin IHC staining, following deparaffinization, antigen retrieval was performed in citrate buffer (pH 6.0) for 10 min. Subsequently, the sections were washed thrice with PBS and the blocking reagent (3% H_2O_2) was mixed at room temperature for 10 min, then incubated overnight with primary antibody (periostin rabbit polyclonal antibody; cat. no. Ap11962b; Abgent Biotech Co., Ltd.; 1:50) at 4˚C. Subsequently, the slides were washed with PBS and incubated with a secondary antibody (goat-anti-rabbit antibodies conjugated to horseradish peroxidase; cat. no. ab6721; Abcam; 1:200) for 30 min at room temperature.

For HIF-1α IHC staining, the slides were deparaffinized and subjected to graded rehydration. Antigen retrieval was performed in citrate buffer (pH 6.0) for 10 min. After washing three times with PBS, the slides were mixed with 3% H_2O_2 at room temperature for 10 min and then incubated overnight with primary antibody (HIF-1α rabbit polyclonal antibody; cat. no. bs-0737R; BIOSS; 1:50) at 4˚C. After washing with PBS, slides were incubated with the secondary antibody (goat-anti-rabbit antibodies conjugated to horseradish peroxidase; cat. no. ab6721; Abcam; 1:200) at room temperature for 30 min. For IHC staining, chromogen detection reagent (DAB horseradish peroxidase color development kit; P0202; Beyotime Institute of Biotechnology) was used.

The staining results were independently assessed by two pathologists under a confocal microscope (Leica TCS SPE, Leica Microsystems GmbH). The pathologists were blinded to the clinical information. The semi-quantitative assessment of the staining intensity was performed using a scale of 0 to 3 as follows: i) 0, no staining; ii) 1, mild staining; iii) 2, moderate staining; and iv) 3, strong staining. The staining area was recorded according to the percentage of positive staining cells as per the following scoring criteria: i) 0, 0%; ii) 1, 1-25%; iii) 2, 26-50%; iv) 3, 51-75%; and v) 4, 76-100%. The final staining score was the sum of the intensity and area scores. Based on the final staining score, the results were categorized into three groups: i) 0-1, negative expression; ii) 2-4, weak expression; and iii) 5-6, strong expression.

Plasmids and transfections. The BCPAP and TPC-1 cells were transfected with lentiviruses containing small hairpin RNA (shRNA) to achieve periostin or HIF-1α silencing. Plasmids of periostin shRNA (cat. no. sc-61324-SH; Santa Cruz Biotechnology, Inc.), HIF-1α shRNA (cat. no. sc-35562-SH; Santa Cruz Biotechnology, Inc.) and control shRNA (cat. no. sc-108060; Santa Cruz Biotechnology, Inc.) were used to knockdown gene expression. All shRNA sequences are listed in Table SII Lentiviruses were produced using a second-generation packaging system. Briefly, 293T cells (cat. no. SNL-015, Wuhan Sunncell Biotech Co., Ltd.) planted in 10-cm dishes were transfected with the respective plenti-shRNA-GFP-Puro vector constructs (10 μg) for shRNA (periostin shRNA, HIF-1α shRNA and control shRNA) together with the packaging vectors, psPAX2 (cat. no. 12260; Addgene; 7.5 μg) and pMD2.G (cat. no. 12259; Addgene; 2.5 μg) using FuGENE 6 transfection reagent (Roche Applied Science). The virus-containing medium was collected twice at 48 and 72 h post-transfection and filtered through a 0.45-μm filter. The lentivirus harvests were concentrated by ultracentrifugation at 110,000 x g for 2 h at 4˚C. Following centrifugation, the supernatant was removed and the precipitate was resuspended in 200 μl Opti-MEM. The BCPAP or TPC-1 cells were then transduced with lentiviral infection at a multiplicity of infection (MOI) of 10 for 24 h (37˚C, 5% CO_2). The GFP fluorescence intensity was monitored under a fluorescent microscope (Olympus CKX41, Olympus Corp.). Transduced cells were screened with puromycin (1 μg/ml) starting at 48 h following transduction. The interference efficiency was confirmed through the detection of mRNA expression. After 5-7 days, resistant polyclonal colonies were further expanded for further analyses (Fig. S1).

To generate the HIF-1α overexpression plasmid, the cDNA encoding HIF-1α was amplified using the following primers: Forward primer, 5'-CAATAGCAGAGCTCTATG GAGGGCGCCGGCGGCGC-3'; and reverse primer, 5'-CCG GTTAGCGCTAGCTCAGTTAACTTGATCCAAAG-3'. The amplified fragment was subcloned into the PLV-304 vector obtained from Asia-vector Biotech, positioned between the *Sac*I (cat. no. R3156L; New England BioLabs, Inc.) and *Nhe*I (cat. no. R3131L; New England BioLabs, Inc.) restriction sites. Following transformation, positive clone colonies were selected for plasmid extraction, and confirmed by sequencing analysis. Subsequently, transfection was performed using Lipofectamine 3000® (cat. no. L3000015; Invitrogen; Thermo Fisher Scientific, Inc.). Briefly, a total of 4x10^{6} 293T cells were plated in 60-mm dishes for 70% fusion on the day of transfection the day before transfection. Transfection reagents containing 2,500 ng HIF-1α overexpression plasmid were prepared and transfected according to the instruction of

manufacturer, and an empty PLV-304 vector was used as a negative control. Cells were harvested after 48 h, RNA was prepared and analyzed using RT-PCR. All cells were cultured in Dulbecco's modified Eagle's High Glucose Medium (DMEM; cat. no. 11965092; Gibco; Thermo Fisher Scientific, Inc.) supplemented with 10% fetal bovine serum (cat. no. A5669701; Gibco; Thermo Fisher Scientific, Inc.), penicillin and streptomycin (cat. no. 15070063; Gibco; Thermo Fisher Scientific, Inc.) at 37°C with 5% CO_2. The interference efficiency was confirmed through the detection of mRNA expression (Fig. S2).

Cell Counting Kit-8 (CCK-8) assay. The cells (BCPAP and TPC-1) were plated in 96-well plates at 200 μl per well and incubated with DMEM containing 10% FBS at 37°C. CCK-8 (BBI Life Sciences Corporation) was used to determine the proliferation of cells at various time points (0, 24, 48 and 72 h). The cells were incubated with 10 μl CCK-8 solution for 1 h at 37°C, and the absorbance at 450 nm was then measured (Biotek EPOCH2, BioTek Instruments, Inc.). Each experiment consisted of five samples. Every independent experiment was performed in triplicate.

MTT assay. The cells (BCPAP and TPC-1) were cultured in 96-well plates at a density of $6x10^3$ cells per well and then cultured for either 3 or 5 days. Cell viability was assessed using MTT assay. Specifically, the cells were incubated with MTT solution (cat. no. M2128; MilliporeSigma) at a concentration of 0.5 mg/ml for 4 h at 37°C. Formaldehyde crystals were dissolved by the addition of dimethyl sulfoxide to each well, and the absorbance at 570 nm was then recorded (Biotek EPOCH2, BioTek Instruments, Inc.). Each experiment consisted of five samples. Every independent experiment was repeated three times.

Transwell migration and invasion assay. Transwell assay was performed to assess the mobility of the cells. The membranes of chamber were coated with (invasion) or without (migration) Matrigel (diluted at 1:8; BD Biosciences) for 2 h at 37°C and cells (BCPAP and TPC-1) were seeded into the top chambers at a density of $2x10^4$ cells/well. The bottom chambers were injected with DMEM containing 10% FBS. Following incubation for 24 h at 37°C, cells invading through membranes were fixed with 4% paraformaldehyde (A500684, BBI Life Sciences Corporation) for 20 min and stained with 0.1% crystal violet (E607309, BBI Life Sciences Corporation) for 30 min at room temperature while non-invading cells on the top chambers were removed. Subsequently, the number of invading cells was counted in six randomly selected visual fields using a fluorescent microscope (Olympus CKX41, Olympus Corporation). Each experiment consisted of three samples. Every independent experiment was repeated three times.

Wound healing assay. The cells (BCPAP and TPC-1) were cultured in a six-well plate at a density of $5x10^5$ cells/well. A scratch wound was drawn by a sterile 200 μl pipette tip after the cells reached 90% confluency. The wells then were then washed with PBS to remove any cellular debris and incubated with 5% CO_2 at 37°C without serum. The distance of cell migration was measured by determining the scratch distance at 0 and 24 h under an inverted microscope (IX71/IX51, Olympus Corporation) using ImageJ software v1.6.0 (National Institutes of Health) on mac OS (16). The quantification of cell migration was determined according the following method: % Migration area=[(area of original wound-area of wound after healing)/area of original wound] x100. Each experiment consisted of three samples. Every independent experiment was repeated three times.

Reverse transcription-quantitative polymerase chain reaction (RT-qPCR). RT-qPCR was performed and total RNA was extracted from the BCPAP cells using TRIzol® reagent (Thermo Fisher Scientific, Inc.). Complementary DNA was synthesized using the Reverse Transcription System kit (Promega Corporation) according to the manufacturer's instructions. qPCR was performed using SG Fast qPCR Master Mix [B639273, Sangon Biotech (Shanghai) Co., Ltd.] and Ex Taq™ kit (DRR100A, Takara Biotechnology Co., Ltd.). cDNA was amplified with the primer sequences for: HIF-1α forward, 5'-ATCCATGTGACCATGAGGAAA TG-3' and reverse, 5'-TCGGCTAGTTAGGGTACACTT C-3'; 125 bp; periostin forward, 5'-CTCATAGTCGTATCA GGGGTCG-3' and reverse, 5'-ACACAGTCGTTTTCTGTC CAC-3'; 138 bp; GAPDH forward, 5'-GGAGCGAGATCC CTCCAAAAT-3' and reverse, 5'-GGCTGTTGTCATACT TCTCATGG-3'; 197 bp. The cycling conditions were 95°C for 3 min for denaturation; followed by 45 cycles of 95°C for 7 sec, 57°C for 10 sec, and 72°C for 15 sec. Relative mRNA expression data were calculated following normalization to GAPDH mRNA and were evaluated using the $2^{-\Delta\Delta Cq}$ method (17) with β-actin as an internal control. Each group consisted of three samples. Every independent experiment was repeated three times.

Western blot analysis. The BCPAP cells were lysed using RIPA lysis buffer [cat. no. KWB002; KIGENE (http://www.kejiebio.com/teamview_3566001.html)] and protein concentration was measured using a BCA kit [cat. no. KWB011; KIGENE (http://www.kejiebio.com/teamview_6783022.html)]. A total of 20 μg protein was loaded on a 10% SDS gel, resolved using SDS-PAGE, and transferred to a PVDF membrane (cat. no. IPVH00010; Millipore). After blocking the non-specific site with blocking reagent [cat. no. KWB023-100; KIGENE (http://www.kejiebio.com/teamview_6479337.html)] for 2 h at room temperature, the membranes were incubated overnight with primary antibodies at 4°C followed by incubation with corresponding secondary antibodies at room temperature for 1 h. The membranes were visualized with the Odyssey Infrared Imaging System (LI-COR Biosciences). The primary antibodies used were as follows: Anti-HIF1α rabbit monoclonal antibody (cat. no. ab51608; Abcam; 1:500); anti-E-cadherin rabbit monoclonal antibody (cat. no. ab76319; Abcam; 1:1,000), anti-N-cadherin mouse monoclonal antibody (cat. no. ab98952; Abcam; 1:1,000); anti-periostin rabbit polyclonal antibody (cat. no. ab79946; Abcam; 1:500); anti-solute carrier family 5 member 5 (NIS) rabbit polyclonal antibody (cat. no. ab240588; Abcam; 1:1,500); anti-GAPDH mouse monoclonal antibody (cat. no. ab8245; Abcam; 1:1,000). The secondary antibodies were anti-mouse (cat. no. ab6728,

Abcam; 1:4,000) or anti-rabbit (cat. no. ab6721, Abcam; 1:4,000) antibodies and were conjugated to horseradish peroxidase. Protein bands were observed using ECL reagent (cat. no. KWB032, Shanghai kejie Biotechnology Co., Ltd.). Each group consisted of eight samples. Every independent experiment was repeated three times.

Chromatin immunoprecipitation (ChIP). ChIP assay was performed by using a kit (MilliporeSigma; cat. no. 17-295), according to the manufacturer's instructions. The BCPAP cells were inoculated in a dish with a diameter of 10 cm at the density of $1x10^7$ cells. A concentration of 37% formaldehyde was added to the BCPAP cells. The protein was lysed using 400 μl of 1% SDS lysate and centrifuged at 19,480 x g at 4°C for 10 min. Normal mouse IgG (cat. no. c2110; Applygen; 1:2,000) as a negative control, or HIF-1α (cat. no. ab243860; Abcam; 1:1,000) antibodies were applied to immunoprecipitated chromatin samples. Subsequently, RT-qPCR was performed by using four primer sets for putative HIF-1α binding sites in the periostin promoter. The sequences of primers 1 to 4 for the periostin promoter were as follows: Primer 1 forward, 5'-TGTGGTTTCACTGTGTGCTT-3' and reverse, 5'-TGGGAAGGCTTTAGGGGAAC-3'; primer 2 forward, 5'-ACCATTTCAGCTCATTGTTTCCC-3' and reverse, 5'-CCTAGCCAAAGGAATGTGCGT-3'; primer 3, forward 5'-TTTTGGCAATGTCCATGTTTCCTA-3' and reverse, 5'-TGCAGCACATCTACTGATAACCA-3'; primer 4 forward, 5'-TCTACTCTGGAAAGGATTGCAGAA-3' and reverse, 5'-GGAACACATTGAGCTACTTTTCCT-3'. Each experiment consisted of three samples. Every independent experiment was performed in triplicate.

Dual luciferase reporter assay. The 293T cells (cat. no. SNL-015, Wuhan Sunncell Biotech Co., Ltd.) were co-transfected with periostin-promoter-WT (wild-type) or periostin-promoter-mut (mutant-type) and HIF-1α over-expression plasmid using Lipofectamine 2000® (Thermo Fisher Scientific, Inc.). The plasmids were purchased from Asia-Vector Biotechnology, Co. Ltd. (http://www.asiavectorbio.cn/gongsijianjie/). Lysates of the cells were incubated at 37°C for 72 h following transfection. Subsequently, Firefly and *Renilla* luciferase activities were measured using the dual luciferase reporter gene detection kit (Promega Corporation; cat. no. E1910) according to the manufacturer's instructions. Each experiment consisted of three samples. Each independent experiment was performed in triplicate.

Determination of adenosine triphosphate (ATP) and lactate dehydrogenase (LDH) content. The ATP and LDH contents were evaluated using the corresponding content detection kit (Nanjing Jiancheng Bioengineering Institute) according to the manufacturer's instructions. The BCPAP cells were added to 96-well plates and incubated at 37°C for 48 h. Subsequently, luminescence reagent was added, and the cells were incubated for 30 min at 37°C. Then luminescence was observed using GloMax Discover (Promega Corporation) while standard curves were established with ATP or LDH standards. The ATP or LDH content was calculated by reading luminescence intensity according to the standard curves. Each independent experiment was performed in triplicate.

Oxygen consumption rate (OCR) and extracellular acidification rate (ECAR) assays. The Seahorse extracellular flux analyzer (cat. no. XF96; Agilent Technologies, Inc.) was employed to assess OCR and ECAR. In brief, the BCPAP cells were seeded in XF96 Seahorse plates at a density of $2x10^4$ cells per well and pre-treated with 100 μM ferric ammonium citrate or deferoxamine at 37°C for 12 h before analysis. Subsequently, 10 mM glucose, 1 μM oligomycin, and 100 mM 2-deoxyglucose were added at specific time points for ECAR measurement by Seahorse analyzer. For OCR measurement, sequential additions of 1 μM oligomycin, 0.5 μM carbonyl cyanide 4-(trifluoromethoxy) phenylhydrazone and 1 μM rotenone/antimycin A were added. Following the Seahorse assays, the results were normalized to cell number, and each independent experiment was repeated three times.

Statistical analysis. All of the statistical analyses were performed using SPSS V.20.0 for Mac (IBM Corp.). Quantitative data are presented as the mean ± standard error of mean (mean ± SEM) and differences between groups were assessed using the Student's t-test (unpaired, two-tailed). Multi-group comparisons were conducted using one-way analysis of variance followed by Tukey's honestly significant difference post-hoc test. The Chi-squared test (two-tailed) and Fisher's exact test were used for the comparison of categorical variables in the IHC data. $P<0.05$ was considered to indicate a statistically significant difference. Prism 8.0 software (GraphPad Software, Inc.) was used to prepare the graphs.

Results

Periostin and HIF-1α expression in TC. The expression levels of periostin and HIF-1α in 95 paired samples of papillary TC and adjacent normal thyroid tissues were assessed using IHC of paraffin slides. As presented in Fig. 1A, periostin was localized in the cytoplasm and demonstrated strong staining in epithelial cancer cells. Periostin expression was upregulated in TC tissues, as compared with normal thyroid tissues, with 52 cases exhibiting a weak expression and 43 cases a strong expression; by contrast, only 14 cases exhibited a weak expression and 81 a negative expression in normal thyroid tissue ($P<0.01$; Fig. 1B). Similar to periostin, HIF-1α also exhibited a higher expression in TC tissues than in normal tissues (Fig. 1C), with 10 cases exhibiting a negative expression, 63 a weak expression and 22 a strong expression; by contrast, 74 cases exhibited a negative expression and 21 a weak expression in normal tissues ($P<0.01$; Fig. 1D). In the 22 cases demonstrating a strong expression of HIF-1α, 20 cases simultaneously exhibited a strong expression of periostin. In addition, the HIF-1α-negative cases exhibited a weak expression of periostin (data not shown). In Fig. 1E, the coexistence of HIF-1α and periostin strong expression in the adjacent sections of the same tissue is presented.

Hypoxia upregulates the expression of periostin in TCs via HIF-1α. A previous study by the authors demonstrated the upregulated expression of periostin mRNA in the BCPAP cell line (9). The BCPAP cell line is a TC cell line with BRAF V600E mutation and exhibit poor biological behavior, and the authors' team have experience using BCPAP cells in a previous study (15). Thus, the BCPAP cell line was used for the
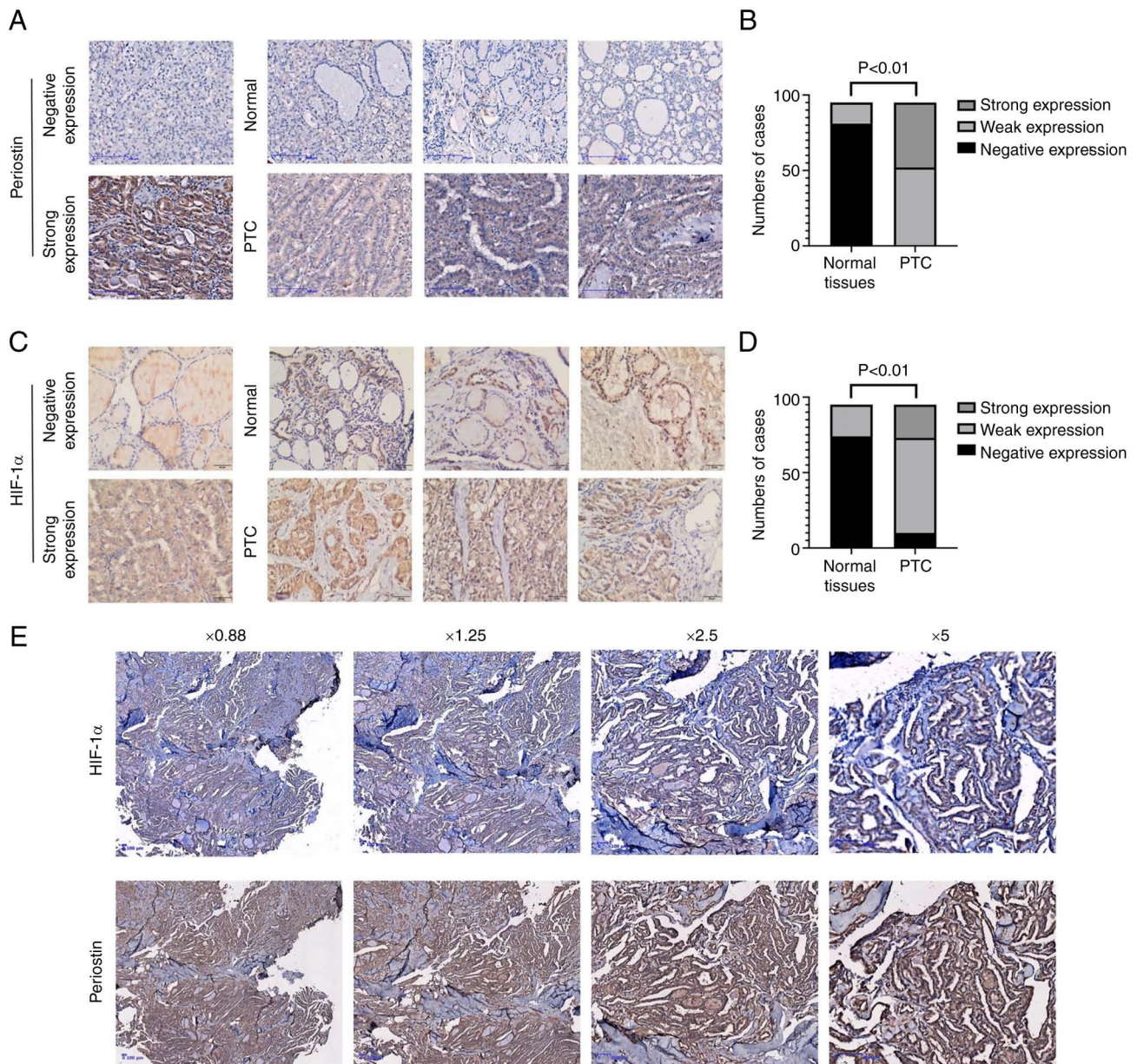
Figure 1. Periostin and HIF-1α expression in thyroid cancer. (A) Periostin protein was localized in the cytoplasm of the cancer cells and in some normal thyroid cells, but with strong staining in the epithelial cancer cells. Brown color indicates periostin positivity, Scale bars, 25 μm. (B) PTC tissues exhibited a significantly higher expression of periostin as compared to normal thyroid tissues (P<0.01). Brown color indicates periostin positivity. (C) HIF-1α was localized in the cytoplasm of cancer cells and some normal thyroid cells, but with strong staining in the cancer cells. Brown color indicates HIF-1α positivity. Scale bars, 20 μm. (D) PTC tissues present with significantly higher expression of HIF-1α, as compared to normal thyroid tissues (P<0.01). (E) Images depicting the staining for HIF-1α and periostin were obtained from adjacent sections of the same tissue at varying magnifications. Scale bars, 25 μm. HIF-1α, hypoxia inducible factor 1 subunit α; PTC, papillary thyroid cancer.

investigation of regulatory mechanisms of periostin expression in TC. To assess the effects of hypoxia on TC cells and the biological role of the hypoxia-HIF-1α-periostin axis in TCs, the BCPAP cells were cultured under normoxic (20% O_2) or hypoxic (1% O_2) conditions separately. The HIF-1α and periostin mRNA levels in the BCPAP cells were assessed using RT-qPCR under normoxic (20% O_2) and hypoxic (1% O_2) conditions, with or without transfection with periostin shRNA. The mRNA expression of HIF-1α in the BCPAP cells under hypoxic conditions was significantly higher in comparison to that under normoxic conditions (P<0.05). In comparison to the BCPAP cells transfected with periostin shRNA under normoxic conditions, the HIF-1α mRNA expression level in

the BCPAP cells was significantly higher following transfection with periostin shRNA under hypoxic conditions (Fig. 2A). The mRNA expression of periostin in the BCPAP cells under hypoxic conditions was significantly higher than that under normoxic conditions (P<0.01). The mRNA expression of periostin significantly decreased following transfection with periostin shRNA under normoxic conditions (P<0.05). Additionally, in comparison to the cells transfected with periostin shRNA under normoxic conditions, the periostin mRNA expression level in the BCPAP cells significantly increased following transfection with periostin shRNA under hypoxic conditions (P<0.01; Fig. 2B). Subsequently, the HIF-1α and periostin mRNA levels were examined using quantitative
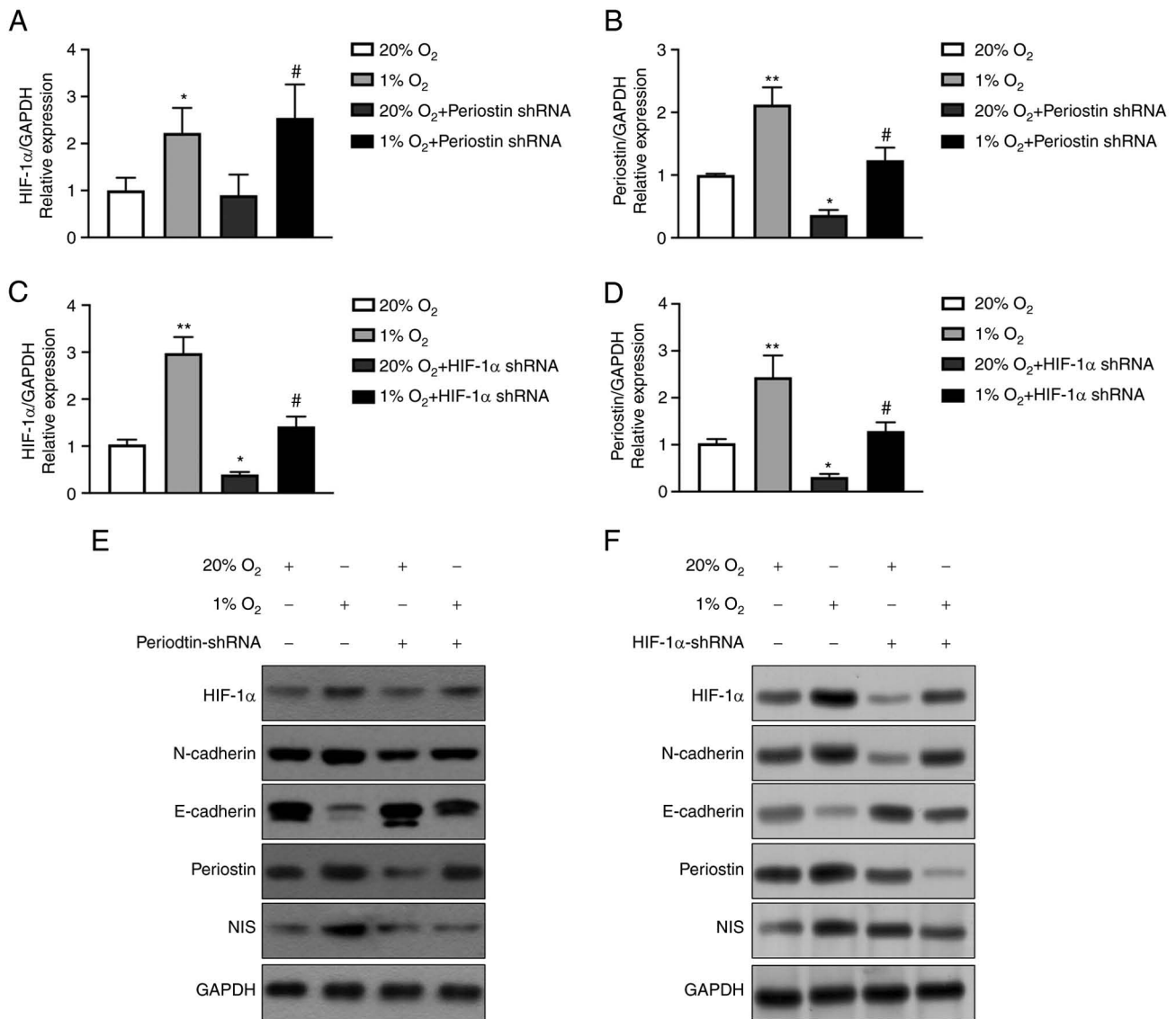
Figure 2. Hypoxia upregulates the expression of periostin in TC cells via HIF-1α. (A) Results of RT-qPCR analysis: the expression of HIF-1α mRNA in BCPAP cells under hypoxic conditions for 24 h was significantly greater than that under normoxic conditions (*P<0.05). Compared to transfection with periostin shRNA under normoxic conditions, the mRNA expression of HIF-1α in BCPAP cells significantly increased with periostin shRNA transfection under hypoxic conditions ($^\#$P<0.05). n=3 biological replicates. Error bars represent standard deviation. (B) Results of RT-qPCR analysis: The mRNA expression of periostin in BCPAP cells under hypoxic conditions for 24 h was significantly greater than that under normoxic conditions (**P<0.01). The mRNA expression of periostin significantly decreased following transfection with periostin shRNA under normoxic conditions (*P<0.05). As compared to transfection with periostin shRNA under normoxic conditions, the mRNA expression of periostin in the BCPAP cells significantly increased following periostin shRNA transfection under hypoxic conditions ($^\#$P<0.01). n=3 biological replicates. Error bars represent standard deviation. (C) Results of RT-qPCR analysis: The expression of HIF-1α mRNA in BCPAPs under hypoxic conditions for 24 h is significantly greater as compared normoxia (**P<0.01). The expression of HIF-1α mRNA significantly decreased following transfection with HIF-1α shRNA under normoxic conditions (*P<0.01). Compared to transfection with HIF-1α shRNA under normoxic conditions, the mRNA expression of HIF-1α in BCPAP cells increased following transfection with HIF-1α shRNA under hypoxic conditions ($^\#$P<0.01). n=3 biological replicates. Error bars represent standard deviation. (D) Results of RT-qPCR analysis: The mRNA expression of periostin in BCPAP cells under hypoxic conditions for 24 h was significantly greater than under normoxic conditions (**P<0.01). The expression of periostin mRNA significantly decreased following the transfection of HIF-1α shRNA under normoxic conditions (*P<0.05). As compared to transfection with HIF-1α shRNA under normoxic conditions, the mRNA expression of periostin in the BCPAP cells significantly increased following transfection with HIF-1α shRNA under hypoxic conditions ($^\#$P<0.01). n=3 biological replicates. Error bars represent standard deviation. (E) Western blot analysis of HIF-1α, N-cadherin, E-cadherin, periostin and NIS under normoxic or hypoxic conditions, with or without periostin shRNA transfection. (F) Western blot analysis of HIF-1α, N-cadherin, E-cadherin, periostin and NIS under normoxic or hypoxic conditions, with or without HIF-1α shRNA transfection. TC, thyroid cancer; HIF-1α, hypoxia inducible factor 1 subunit α; RT-qPCR, reverse transcription-quantitative polymerase chain reaction; NIS, solute carrier family 5 member 5.

RT-qPCR in the BCPAP cells under normoxic (20% O$_2$) and hypoxic (1% O$_2$) conditions, with or without transfection with HIF-1α shRNA. The results presented in Fig. 2C demonstrate that hypoxia significantly increased the expression of HIF-1α (P<0.01) and transfection with HIF-1α shRNA attenuated this effect (P<0.01). At the same time, hypoxic conditions

also induced a significant increase in periostin expression (P<0.01). However, transfection with HIF-1α shRNA limited the upregulation of periostin expression (P<0.01; Fig. 2D). As demonstrated using western blot analysis, hypoxia increased the protein expression of HIF-1α and periostin, as well as that of the EMT-related proteins, N-cadherin and NIS
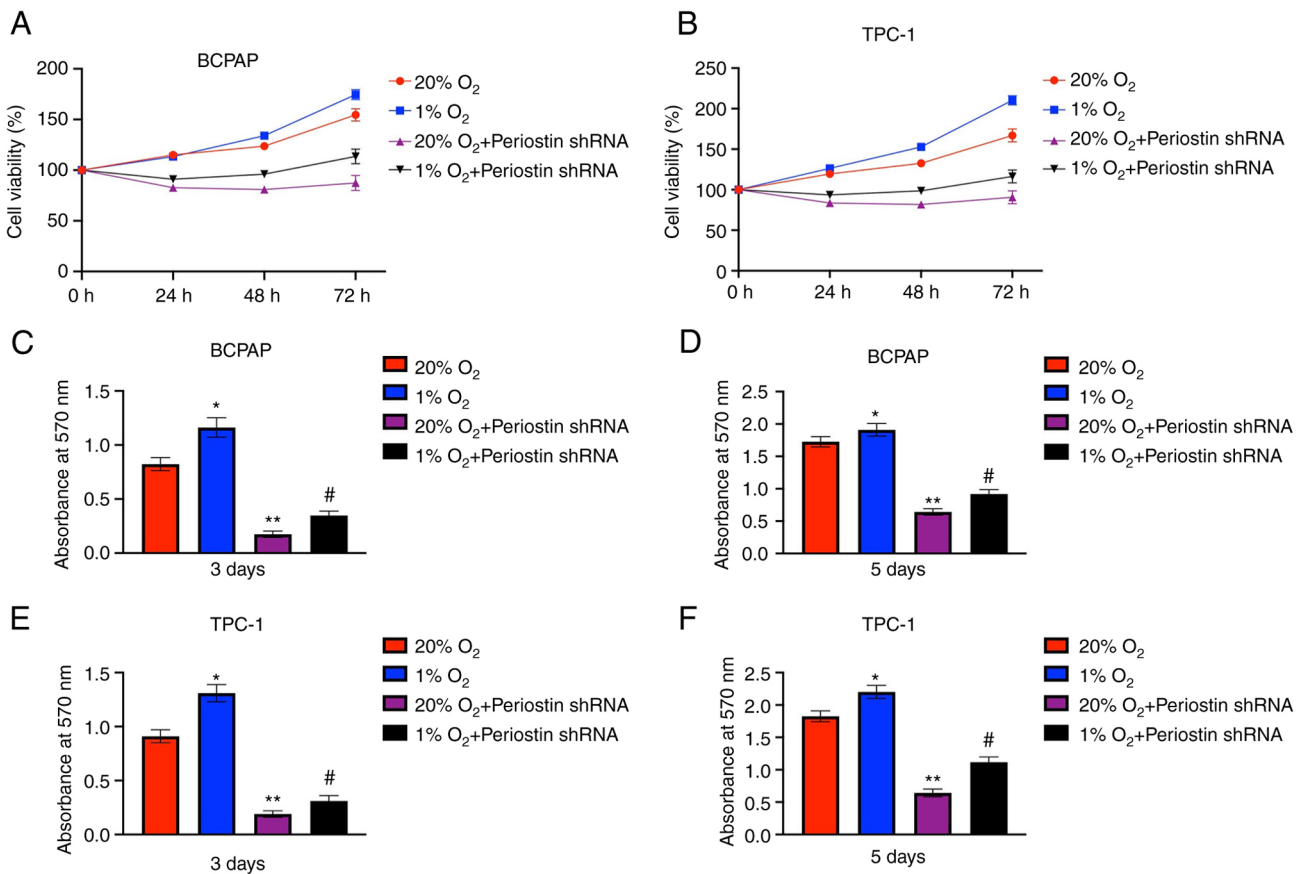
Figure 3. Effects of hypoxia and periostin on the proliferation of TC cells. (A and B) Effects of hypoxia and periostin shRNA on proliferation were evaluated using CCK-8 assays in BCPAP and TPC-1 cells at different time points (24, 48 and 72 h). Results of CCK-8 assay at 72 h show significantly an increased cell proliferation of TC cells (BCPAP and TPC-1) under hypoxic conditions vs. normoxic conditions (P<0.05); transfection with Periostin shRNA inhibited the proliferation of cells (P<0.05). Hypoxia combined with transfection with periostin shRNA inhibited the proliferation of TC cells compared to the cells subjected only to hypoxia (P<0.05). n=3 biological replicates; error bars represent standard deviation. (C-F) Results of MTT assay: Both the BCPAP and TPC-1 cells exhibited a significantly greater proliferation under hypoxic compared with normoxic conditions for 3 and 5 days (*P<0.05); transfection with periostin shRNA inhibited cell proliferation following culture for 3 and 5 days (**P<0.01). Hypoxia combined with periostin shRNA transfection inhibited the proliferation of TC cells compared with the cells subjected only to hypoxia ($^\#$P<0.01). n=3 biological replicates; error bars represent standard deviation. TC, thyroid cancer; CCK-8, Cell Counting Kit-8 assay.

(sodium-iodide symporter), and decreased the expression of E-cadherin. When the cells were transfected with shRNA against periostin, the N-cadherin and NIS level decreased, while that of E-cadherin increased under both normoxic and hypoxic conditions (Fig. 2E). The knockdown of HIF-1α exerted a similar effect on EMT-related proteins and inhibited the protein expression of periostin (Fig. 2F).

Effects of hypoxia and periostin on the proliferation of TC cells. CCK-8 assay was conducted to examine the proliferation of BCPAP and TPC-1 cells. The viability of the BCPAP and TPC-1 cells at different time points (24, 48 and 72 h) of culture under normoxic or hypoxic conditions with or without periostin shRNA transfection is shown in Fig. 3A and B. The results revealed that hypoxia enhanced the viability of the BCPAP cells, while periostin shRNA inhibited the viability of the BCPAP cells under both normoxic and hypoxic conditions. MTT assay also revealed similar results. After culturing for 3 and 5 days, both the BCPAP and TPC-1 cells exhibited a significant elevation in proliferation under hypoxic compared to normoxic conditions; however, transfection with periostin shRNA inhibited the effects of hypoxia (Fig. 3C-F).

Fig. 3C and E demonstrate that when cultured for 72 h, the proliferation of BCPAP and TPC-1 cells under hypoxic conditions was significantly greater than that under normoxic conditions (P<0.05); transfection with periostin shRNA inhibited the proliferation of BCPAP cells (P<0.01). Hypoxia combined with periostin shRNA transfection inhibited the proliferation of BCPAP cells compared to the cells subjected only to hypoxia (P<0.05).

Effect of hypoxia and periostin on the invasion and migration of TC cells. In a previous study by the authors, the knockdown of periostin significantly reduced the invasiveness of BCPAP cells (9). In the present study, Transwell assay was performed to evaluate the effects of the interaction between hypoxia and periostin on the invasion and migration of BCPAP cells. As shown in Fig. 4A and B, the invasiveness and migratory ability of the BCPAP and TPC-1 cells under hypoxic conditions was significantly greater than that under normoxic conditions (P<0.05). The knockdown of periostin following transfection with periostin shRNA markedly inhibited the invasiveness and migratory ability of the cells (P<0.01). Notably, the combination of hypoxia
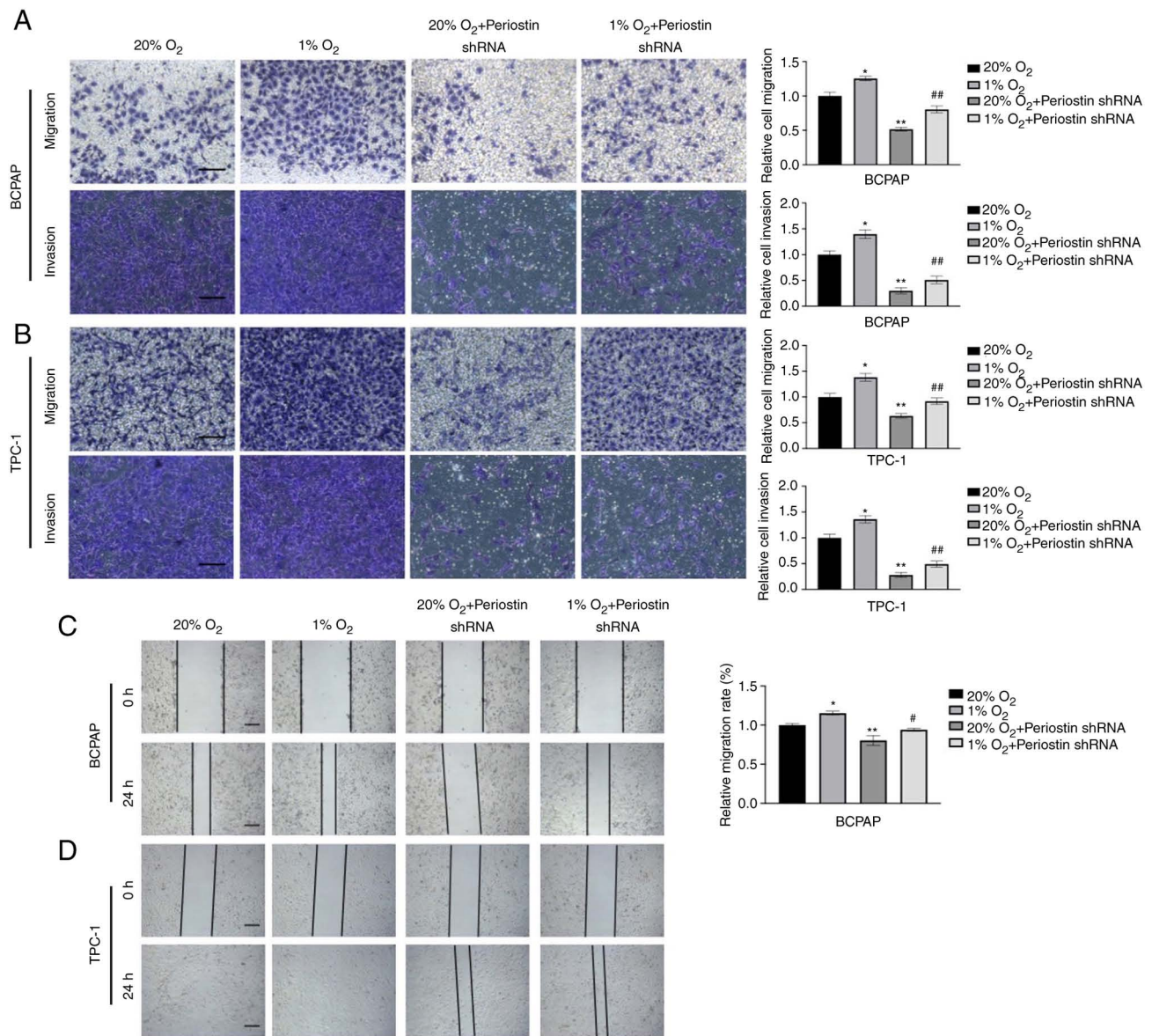
Figure 4. Effects of hypoxia and periostin on the invasiveness and migratory ability of TC cells. (A and B) Transwell migration and invasion assays. BCPAP and TPC-1 cells under normoxic or hypoxic conditions plus transfection with or without periostin shRNA (c-shRNA). The number of cells that migrated or invaded through Matrigel-coated inserts was determined. Invasiveness capability of cells under hypoxic conditions for 24 h was significantly greater than that under normoxic conditions (*P<0.05). Transfection with periostin shRNA inhibited the invasiveness capability of cells (**P<0.01). Hypoxia combined with periostin shRNA transfection restored the invasiveness capability of cells compared to only periostin shRNA transfection (##P<0.01). The migratory capability of cells under hypoxic conditions for 24 h was significantly greater than that under normoxic conditions (*P<0.05). Transfection with periostin shRNA inhibited the migration capability of cells (**P<0.01). Hypoxia combined with periostin shRNA transfection restored the migration capability of cells compared to only periostin shRNA transfection (##P<0.01). Scale bars, 50 µm; n=3 biological replicates. (C and D) Wound healing assay. BCPAP and TPC-1 cells under normoxia or hypoxia plus transfection with or without periostin shRNA. Wound healing assays suggested BCPAP cells under hypoxic conditions achieved an increased healing rate as compared with that under normoxic conditions (*P<0.05); periostin knockdown significantly inhibited this effect (**P<0.05). Hypoxia combined with periostin shRNA remitted the mobility of cells (#P<0.05). Scale bars, 100 µm; n=3 biological replicates. TC, thyroid cancer.

and periostin shRNA transfection remitted the invasiveness and migratory capability of the cells compared with that of the cells transfected with periostin shRNA under normoxic conditions. The results of wound healing assay also suggested the same effect. A more rapid migration was observed in the BCPAP cells under hypoxic conditions, as compared with that under normoxic conditions (P<0.05), and in TPC-1 cells, full confluency was observed under hypoxic conditions, while partial confluency was observed under normoxic conditions. Furthermore, periostin knockdown inhibited the migration in both BCPAP and TPC-1

cells, and hypoxia combined with periostin shRNA remitted the mobility of cells (Fig. 4C and D).

Molecular mechanisms of regulation of periostin expression by HIF-1α. Subsequently, the present study aimed to investigate the underlying molecular mechanisms by which HIF-1α regulates periostin gene expression in TCs. Immunoprecipitation assay and luciferase reporter assay were performed to analyze the human periostin promoter with respect to putative HIF-1α binding sites. The human periostin promoter contains four HIF-1α consensus sequences as potential binding sites, which
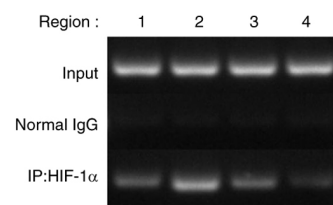
A

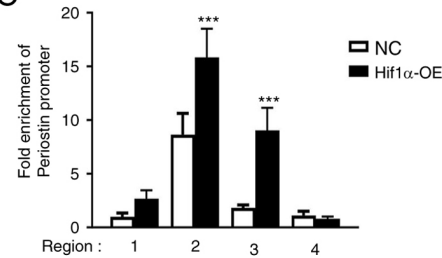| Matrix ID	Name	Score	Relative score	Sequence ID	Start	End	Strand	Predicted sequence
MA0259.1	MA0259.1.ARNT::HIF1A	5.5020556	0.8300451416024047	NC_000013.11:c37600568-37598768	1038	1045	+	AGATGTGC
MA0259.1	MA0259.1.ARNT::HIF1A	4.8468323	0.8104982268281529	NC_000013.11:c37600568-37598768	202	209	+	CCACCTGC
MA0259.1	MA0259.1.ARNT::HIF1A	4.798817	0.8090658184983601	NC_000013.11:c37600568-37598768	993	1000	+	ACACTTGC
MA0259.1	MA0259.1.ARNT::HIF1A	4.762659	0.807987134440166	NC_000013.11:c37600568-37598768	854	861	−	GAATGTGC

Showing 1 to 4 of 4 entries   Previous 1 Next
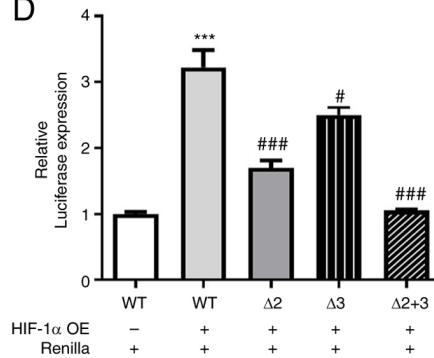

Figure 5. Molecular mechanisms of the regulation of periostin expression by HIF-1α. (A) The human periostin promoter contains four HIF-1α consensus sequences for potential binding sites. (B) DNA agarose gel electrophoresis results of input, control IgG and amplified products by HIF-1α overexpression plasmid from primer 1 to primer 4. (C) The results of reverse transcription-quantitative PCR are presented as regions amplified with four different primer pairs (primer 1-primer 4). The results revealed that binding of HIF-1α in the region probed with primer 2 and primer 3 amplified significantly compared to the control group after HIF-1α overexpression (***P<0.001), and fold enrichment of primer 2 was higher. (D) Luciferase reporter assays results. Compared to the blank control group, periostin-promoter-WT co-transfection with HIF-1α overexpression plasmid significantly increased the luciferase activity (***P<0.001). Co-transfection of mutant periostin-promoter with primer 2 (Δ2 mutant-type) or primer 3 (Δ3 mutant-type) with a HIF-1α overexpression plasmid demonstrated a significantly decreased luciferase activity, as compared with periostin-promoter-WT (#P<0.05 and ###P<0.001). Co-mutant of primer 2 and primer 3 (Δ2+3 mutant-type) resulted the luciferase activity being most significantly decreased ###P<0.001). HIF-1α, hypoxia inducible factor 1 subunit α; WT, wild-type.

were predicted using JASPAR, and are presented in Fig. 5A. Regions amplified with four different primer pairs (primer 1-primer 4) subsequently tested using immunoprecipitation. Immunoprecipitation with BCPAP cells (negative control cells and HIF-1α overexpression cells) was then performed. The results of DNA agarose gel electrophoresis are presented in Fig. 5B, with region 2 demonstrating the highest signal. The quantification of the target DNA was achieved using RT-qPCR and the results are presented in Fig. 5C. Immunoprecipitation analysis revealed that in HIF-1α-overexpressing cells, binding of HIF-1α in region 2 and region 3 was significantly amplified as compared with negative control BCPAP cells (P<0.001), and fold enrichment of region 2 was higher. Additionally, luciferase reporter assay was conducted, in order to further elucidate the mechanisms by which HIF-1α regulates periostin (Fig. 5D). In comparison with the blank control group, the co-transfection of periostin-promoter-wild type (WT) with

HIF-1α overexpression plasmid significantly increased the luciferase activity (P<0.001). Conversely, the co-transfection of the mutant periostin-promoter of Δ2 mutant-type (region 2 deletion mutation) or Δ3 mutant-type (region 3 deletion mutation) with the HIF-1α overexpression plasmid resulted in a significantly decreased luciferase activity, as compared to periostin-promoter-WT (P<0.05). When region 2 and region 3 were simultaneously mutated (Δ2+3 mutant-type), the luciferase activity returned to baseline. These results, combined with the results of immunoprecipitation assay, suggested that HIF-1α increased the periostin levels by binding to the periostin promoter.

Hypoxia induces Warburg effect via upregulation of periostin expression. The Warburg effect refers to the phenomenon wherein cancer cells utilize a significant amount of energy through glycolysis, even in the presence of oxygen, in
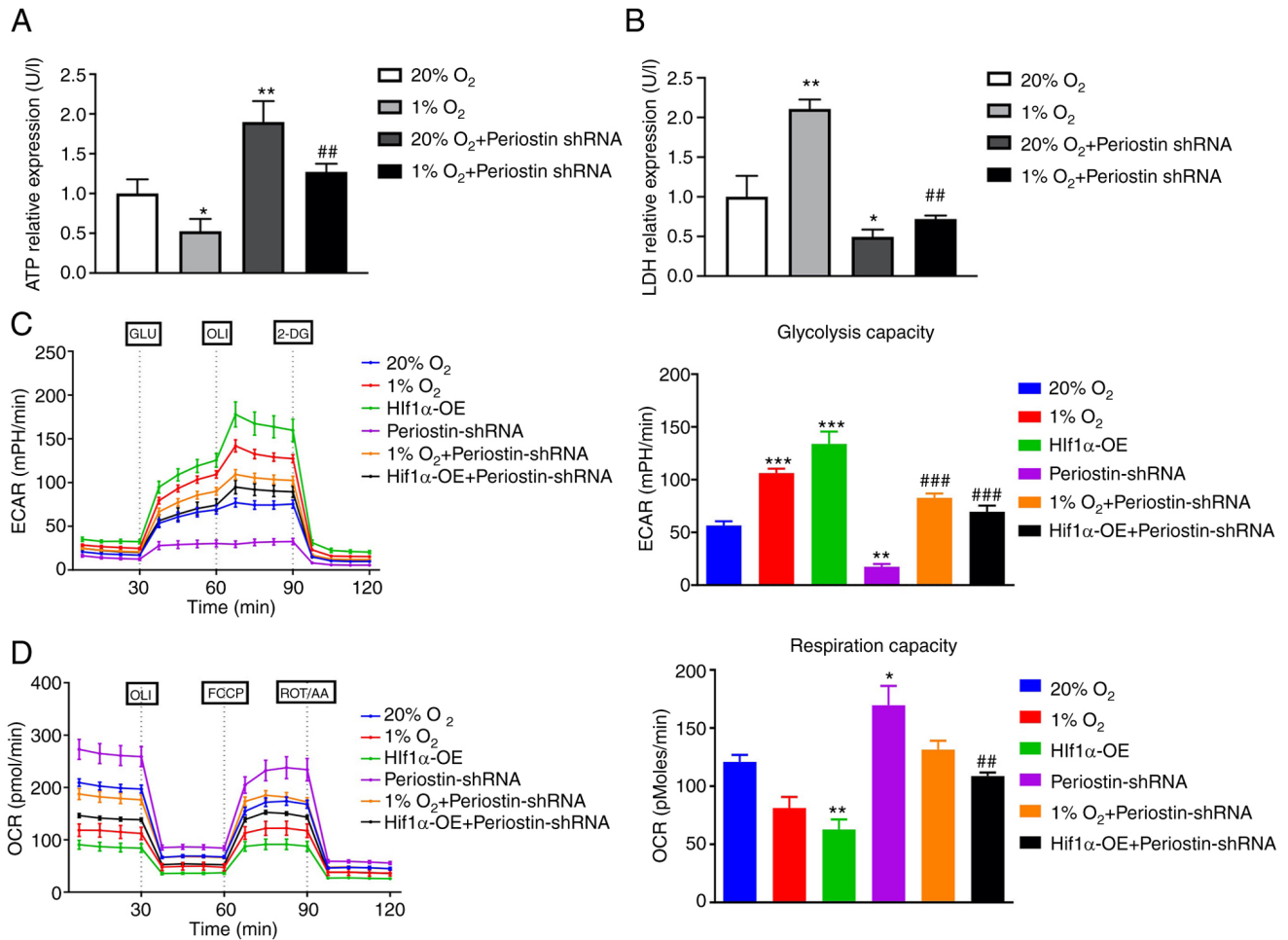
Figure 6. Hypoxia induced the Warburg effect by upregulating the expression of periostin. (A) Results of phosphomolybdic acid colorimetry. ATP expression in BCPAP cells under hypoxic conditions was significantly lower than that under normoxic conditions (*P<0.05). Transfection with periostin shRNA under normoxic conditions increased the ATP expression in BCPAPs (**P<0.01). As compared to the hypoxic group, transfection using periostin shRNA under hypoxic conditions significantly increased the ATP expression in BCPAP cells (##P<0.01). (B) Results of the LDH test. The LDH expression in BCPAPs under hypoxic conditions was significantly higher than that under normoxic conditions (*P<0.05). Transfection with periostin shRNA under normoxic conditions decreased LDH expression in BCPAPs (**P<0.01). In comparison with the hypoxic group, transfection with periostin shRNA under hypoxic conditions significantly decreased LDH expression in BCPAP cells (##P<0.01). (C and D) The ECAR and OCR of BCPAP cells under different conditions were measured using the Seahorse analyzer. The ECAR of BCPAP cells under hypoxic conditions or with HIF-1α overexpression was significantly higher than that under nomoxia (***P<0.001). Transfection with periostin shRNA under normoxic conditions significantly decreased the ECAR of BCPAP cells (**P<0.01). Transfection using periostin shRNA under hypoxic conditions or co-transfection with HIF-1α overexpression plasmids increased the ECAR of BCPAP cells (###P<0.001). By contrast, the OCR of BCPAPs with HIF-1α overexpression was significantly decreased (**P<0.01). Transfection with periostin shRNA significantly elevated the OCR of BCPAP cells (*P<0.05). Transfection with periostin shRNA under hypoxic conditions or co-transfection with HIF-1α overexpression plasmids decreased the OCR of BCPAP cells (##P<0.01 and ###P<0.001, respectively). LDH, lactate dehydrogenase; ECAR, extracellular acidification rate; OCR, oxygen consumption rate; HIF-1α, hypoxia inducible factor 1 subunit α.

order to support their uncontrolled growth (18). Changes in ATP and LDH are key indicators of the switch of cellular metabolism from the tricarboxylic acid cycle to glycolysis. Phosphomolybdic acid colorimetry revealed that the level of ATP in the BCPAP cells was significantly decreased under hypoxic conditions compared to that under normoxic conditions (P<0.05). Transfection with periostin shRNA under normoxic conditions significantly increased the ATP expression in the BCPAP cells (P<0.01). Compared to hypoxic group, transfection with periostin shRNA under hypoxic conditions significantly increased ATP expression in BCPAPs (P<0.01; Fig. 6A). Similarly, LDH expression in BCPAPs under hypoxic conditions was significantly increased in comparison with normoxic conditions (P<0.05). Transfection with periostin shRNA under normoxic conditions significantly decreased

the LDH expression in BCPAPs (P<0.01). Compared to hypoxic group, transfection with periostin shRNA under hypoxic conditions significantly decreased the LDH expression in BCPAPs (P<0.01; Fig. 6B). The ECAR and OCR were further tested by using a Seahorse metabolic analyzer under different conditions in BCPAP cells (20% O₂, 1% O₂, HIF-1α overexpression under 20% O₂, periostin shRNA under 20% O₂, periostin shRNA under 1% O₂ and periostin shRNA plus HIF-1α overexpression under 20% O₂). The results demonstrated that the BCPAP cells under hypoxic conditions or the BCPAP cells transfected with HIF-1α overexpression plasmid significantly increased the ECAR of the cells compared to that under normoxic conditions. Notably, transfection with periostin shRNA significantly decreased the ECAR (P<0.01), reflecting that periostin and HIF-1α may play crucial roles

in TC glycolysis (Fig. 6C). Correspondingly, hypoxia or transfection with HIF-1α overexpression plasmid decreased the OCR of the BCPAP cells as compared to the cells under normoxic conditions and those transfected with periostin shRNA (Fig. 6D). These results indicate that hypoxia may induce the Warburg effect by upregulating periostin expression.

Discussion

The extracellular matrix protein, periostin, is usually expressed at reduced levels in normal adult tissues; however, periostin expression is increased at sites of inflammation, injury and in tumors (19-21). The role of periostin in tumor development and progression has attracted increasing attention in recent years. Periostin has a number of biological functions in tumors, including the regulation of proliferation, invasion, metastasis and angiogenesis.

It has been reported that periostin is secreted by both stromal cells and tumor cells (22-25). A previous study by the authors (9) and the present study demonstrated the overexpression of periostin in human TC cell lines, as well as in human TC tissues. Periostin overexpression in TC has been demonstrated to be related to poor prognostic features, including an advanced tumor stage, extrathyroidal extension, or lymph node metastasis (26-30).

Therefore, in a previous study by the authors, the effects of silencing periostin on the growth, invasion and tumorigenesis of thyroid cancer cells were investigated. Eventually, it was observed that periostin may regulate the growth and progression of TC through the Akt/thyroid stimulating hormone receptor axis (9). In the present study, the role of periostin in the development of TC was further explored and an attempt was made to identify the regulator of periostin.

HIF-1 is a transcription factor that plays a crucial role in cellular response to hypoxia. Under normoxic conditions, HIF-1 is hydroxylated and targeted for degradation (31-33). However, under hypoxic conditions or in the context of activated RTK pathways, the hydroxylation is inhibited, leading to HIF-1 accumulation in the nucleus. Once in the nucleus, HIF-1 functions as a transcription factor, binding to hypoxia response elements in the promoter region of target genes (34,35). HIF-1 target genes include those involved in angiogenesis, e.g., vascular endothelial growth factor (36); glucose metabolism, e.g., pyruvate dehydrogenase kinase 1 (37) and cell survival, e.g., p53 (38), which are essential for adaptation to low oxygen conditions.

Periostin expression has been revealed to be induced by inflammation or mechanical stress. However, the impact of hypoxia on periostin has not yet been fully elucidated (39). Malignances are known to be characterized by changes in energy metabolism. Srinivasan et al (40) demonstrated the involvement of periostin in the pathway inducing the metabolic shift to glycolysis in esophageal squamous cell carcinoma and breast cancer.

The effect of the hypoxia-HIF-1α-periostin axis has been revealed in various processes of wound healing. The study by Zhang et al (41) suggested that in keloid fibroblasts, hypoxia-induced periostin overexpression was regulated by HIF-1α. In the study by Aukkarasongsup et al (42),

periostin silencing was reported to inhibit tge hypoxia-induced apoptosis of human periodontal ligament cells. In addition to the context of wound healing, the role of the hypoxia-HIF-1α-periostin axis in tumor progression has attracted increasing attention in recent years. In the present study, hypoxia was observed to promote the viability and invasion of TC cells, with these effects being inhibited by the knockdown of periostin. Subsequently, it was observed that hypoxia upregulated the expression of periostin via HIF-1α, both at the mRNA and protein level, preliminarily establishing the hypoxia-HIF-1α-periostin axis in TC. This result was consistent with the findings of the study by Guo et al (43), in which the exposure of glioma cells to hypoxia led to an increased expression of periostin and HIF-1α. In the study by Liu et al (44), HIF-1α depletion blocked the hypoxia-induced upregulation of periostin expression in hepatocellular carcinoma cells.

The Warburg effect, also known as aerobic glycolysis, is a phenomenon observed in cancer cells wherein glycolysis is preferentially used for energy production even in the presence of oxygen. This metabolic adaptation allows cancer cells to rapidly generate energy and biosynthetic precursors required for cell proliferation and viability, thus allowing cells to maintain energy production despite reduced oxygen availability. The increased glycolytic flux not only provides ATP but also metabolic intermediates that can be used for various biosynthetic pathways involved in cell proliferation and activity (10,18,45). In the present study, lactate and ATP concentrations were measured under different conditions and the ECAR and OCR of BCPAP cells were tested under different conditions. The results revealed that in TC cells, periostin plays a crucial role in the Warburg effect. Similar to the findings of the present study, Yang et al (46) demonstrated the involvement of the Warburg effect in the promotion of tumorigenesis in TC; however, their study focused on the association between the Warburg effect and autophagy.

Under hypoxic conditions, the accumulation of reactive oxygen species may lead to mitochondrial damage, subsequently resulting in cell death (47). HIF-1 serves to induce a process known as mitophagy, entailing the removal of impaired mitochondria to prevent them from causing harm to cells (48). The pathways mediating mitophagy can be categorized into ubiquitin-dependent (Ub-dependent) and ubiquitin-independent (Ub-independent) pathways. The Ub-dependent pathway predominantly involves the PTEN induced kinase 1/Parkin signaling pathway (49), while Ub-independent pathways, such as the FUN14 domain containing 1 pathway (50,51), have been reported to play a crucial role in tumor progression. HIF-1α triggers mitophagy to protect hypoxic cells from damage. On the other hand, the Warburg effect is consequently induced, shifting oxidative metabolism toward glycolysis to reduce oxygen demand and maintain normal energy supply (18). This regulatory role of HIF-1 in cell metabolism plays a pivotal role in ensuring the survival and progression of tumor cells under hypoxic conditions. In a previous study by the authors, hypoxia and the overexpression of periostin led to an increase in LC3 levels (9). In future studies, the authors aim to further investigate the interactions between the hypoxia-HIF-1α-periostin axis and pathways associated with mitophagy.
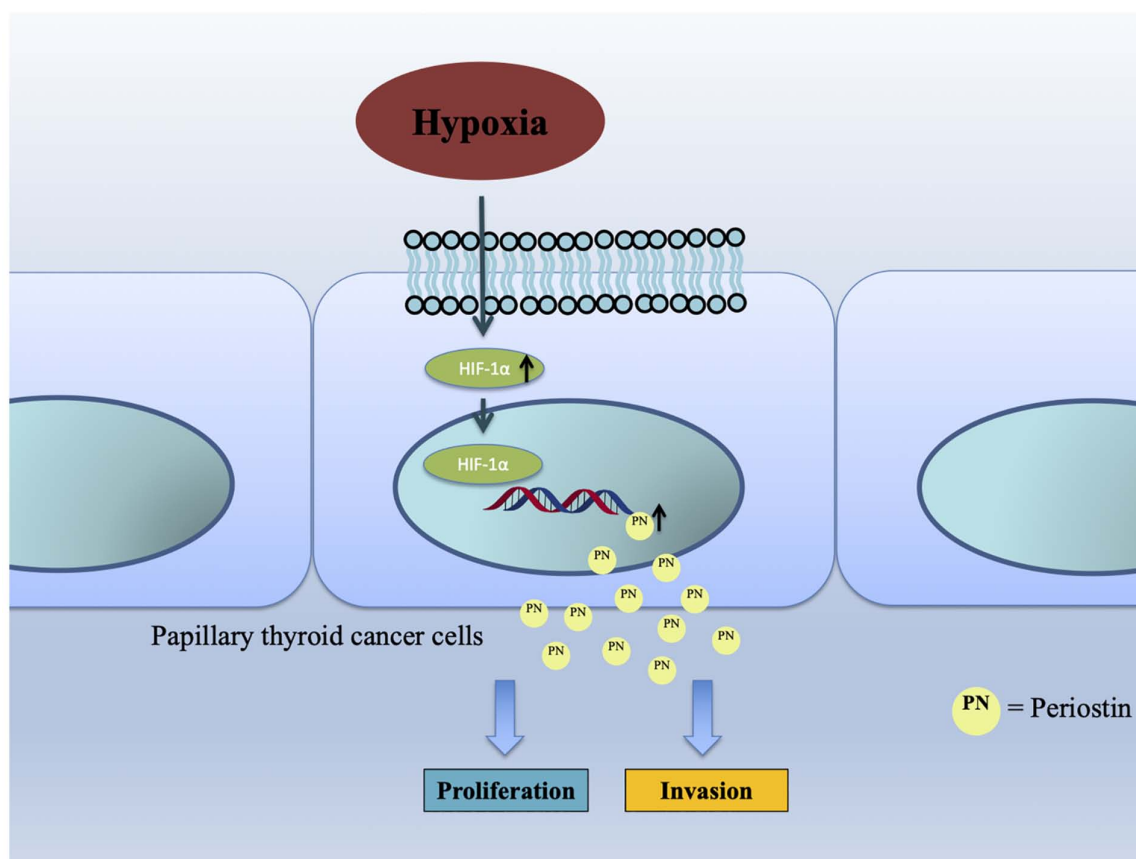
Figure 7. Schematic representation of the effect of hypoxia-HIF-1α-periostin axis in thyroid cancer. HIF-1α, hypoxia inducible factor 1 subunit α.

However, the mechanisms by which HIF-1α regulates periostin remain unclear. Using informatics tools, it was predicted that HIF-1α may potentially bind to the promoter of periostin. Subsequent immunoprecipitation and dual luciferase reporter assays revealed that HIF-1α induced by hypoxia upregulated the expression of periostin through binding to the promoter of periostin. Therefore, HIF-1α and periostin are potential biomarkers and therapeutic targets in the context of TC.

The findings of the present study demonstrate the existence of the hypoxia-HIF-1α-periostin axis in TC and suggest its role in the progression of TC. Hypoxia was found to induce the Warburg effect in TC and periostin was suggested to be involved in the regulation of metabolism in TC.

In conclusion, the findings of the present study demonstrated the impact of the hypoxia-induced activation of periostin via the HIF-1α pathway on the viability and migration of TC cells, as well as the Warburg effect in TC (Fig. 7). These findings may provide potential therapeutic targets in the context of TC.

Acknowledgements

Not applicable.

Funding

Availability of data and materials

The datasets used and/or analyzed during the current study are available from the corresponding author on reasonable request.

Authors' contributions

YY and MW conceived and designed the study, and drafted the manuscript. JW, HZ and JL performed the experiments. YL and XS collected patient specimens and performed the statistical analysis. All authors have read and approved the final manuscript. YY and MW confirm the authenticity of all the raw data.

Ethics approval and consent to participate

The present study was approved by the Ethics Committee for Clinical Research of Shanghai General Hospital, Shanghai Jiaotong University School of Medicine (Approval no. 2019KY016). Written informed consent was obtained from all patients included in the study.

Patient consent for publication

Not applicable.

Competing interests

The authors declare that they have no competing interests.

References

1. Wang J, Yu F, Shang Y, Ping Z and Liu L: Thyroid cancer: Incidence and mortality trends in China, 2005-2015. Endocrine 68: 163-173, 2020.
2. La Vecchia C, Malvezzi M, Bosetti C, Garavello W, Bertuccio P, Levi F and Negri E: Thyroid cancer mortality and incidence: A global overview. Int J Cancer 136: 2187-2195, 2015.
3. Hughes DT, Haymart MR, Miller BS, Gauger PG and Doherty GM: The most commonly occurring papillary thyroid cancer in the United States is now a microcarcinoma in a patient older than 45 years. Thyroid 21: 231-236, 2011.
4. Lim H, Devesa SS, Sosa JA, Check D and Kitahara CM: Trends in thyroid cancer incidence and mortality in the United States, 1974-2013. JAMA 317: 1338-1348, 2017.
5. Ibrahimpasic T, Ghossein R, Shah JP and Ganly I: Poorly differentiated carcinoma of the thyroid gland: Current status and future prospects. Thyroid 29: 311-321, 2019.
6. Dettmer MS, Schmitt A, Komminoth P and Perren A: Poorly differentiated thyroid carcinoma: An underdiagnosed entity. Pathologe 41 (Suppl 1): S1-S8, 2020.
7. González-González L and Alonso J: Periostin: A matricellular protein with multiple functions in cancer development and progression. Front Oncol 8: 225, 2018.
8. Liu Y, Huang Z, Cui D and Ouyang G: The multiaspect functions of periostin in tumor progression. Adv Exp Med Biol 1132: 125-136, 2019.
9. Wang M, Gui C, Qiu S, Tang J and Peng Z: Periostin silencing suppresses the aggressive phenotype of thyroid carcinoma cells by suppressing the Akt/thyroid stimulating hormone receptor axis. Cytotechnology 70: 275-284, 2018.
10. Schwartz L, Supuran CT and Alfarouk KO: The Warburg effect and the hallmarks of cancer. Anticancer Agents Med Chem 17: 164-170, 2017.
11. Wang HJ, Hsieh YJ, Cheng WC, Lin CP, Lin YS, Yang SF, Chen CC, Izumiya Y, Yu JS, Kung HJ, et al: JMJD5 regulates PKM2 nuclear translocation and reprograms HIF-1α-mediated glucose metabolism. Proc Natl Acad Sci USA 111: 279-284, 2014.
12. Semenza GL: HIF-1 and mechanisms of hypoxia sensing. Curr Opin Cell Biol 13: 167-171, 2001.
13. Semenza GL: Hypoxia-inducible factor 1 (HIF-1) pathway. Sci STKE 2007: cm8, 2007.
14. Kierans SJ and Taylor CT: Regulation of glycolysis by the hypoxia-inducible factor (HIF): Implications for cellular physiology. J Physiol 599: 23-37, 2021.
15. Schweppe RE, Klopper JP, Korch C, Pugazhenthi U, Benezra M, Knauf JA, Fagin JA, Marlow LA, Copland JA, Smallridge RC and Haugen BR: Deoxyribonucleic acid profiling analysis of 40 human thyroid cancer cell lines reveals cross-contamination resulting in cell line redundancy and misidentification. J Clin Endocrinol Metab 93: 4331-4341, 2008.
16. Rueden CT, Schindelin J, Hiner MC, DeZonia BE, Walter AE, Arena ET and Eliceiri KW: ImageJ2: ImageJ for the next generation of scientific image data. BMC Bioinformatics 18: 529, 2017.
17. Livak KJ and Schmittgen TD: Analysis of relative gene expression data using real-time quantitative PCR and the 2(-Delta Delta C(T)) method. Methods 25: 402-408, 2001.
18. Vander Heiden MG, Cantley LC and Thompson CB: Understanding the Warburg effect: The metabolic requirements of cell proliferation. Science 324: 1029-1033, 2009.
19. Sonnenberg-Riethmacher E, Miehe M and Riethmacher D: Periostin in allergy and inflammation. Front Immunol 12: 722170, 2021.
20. Ratajczak-Wielgomas K and Dziegiel P: The role of periostin in neoplastic processes. Folia Histochem Cytobiol 53: 120-132, 2015.
21. Yamaguchi Y: Periostin in skin tissue and skin-related diseases. Allergol Int 63: 161-170, 2014.
22. Kudo Y, Iizuka S, Yoshida M, Nguyen PT, Siriwardena SB, Tsunematsu T, Ohbayashi M, Ando T, Hatakeyama D, Shibata T, et al: Periostin directly and indirectly promotes tumor lymphangiogenesis of head and neck cancer. PLoS One 7: e44488, 2012.
23. Zhang Y, Zhang G, Li J, Tao Q and Tang W: The expression analysis of periostin in human breast cancer. J Surg Res 160: 102-106, 2010.
24. Utispan K, Thuwajit P, Abiko Y, Charngkaew K, Paupairoj A, Chau-in S and Thuwajit C: Gene expression profiling of cholangiocarcinoma-derived fibroblast reveals alterations related to tumor progression and indicates periostin as a poor prognostic marker. Mol Cancer 9: 13, 2010.
25. Kikuchi Y, Kunita A, Iwata C, Komura D, Nishiyama T, Shimazu K, Takeshita K, Shibahara J, Kii I, Morishita Y, et al: The niche component periostin is produced by cancer-associated fibroblasts, supporting growth of gastric cancer through ERK activation. Am J Pathol 184: 859-870, 2014.
26. Kusafuka K, Yamashita M, Iwasaki T, Tsuchiya C, Kubota A, Hirata K, Murakami A, Muramatsu A, Arai K and Suzuki M: Periostin expression and its supposed roles in benign and malignant thyroid nodules: An immunohistochemical study of 105 cases. Diagn Pathol 16: 86, 2021.
27. Giusca SE, Amalinei C, Lozneanu L, Ciobanu Apostol D, Andriescu EC, Scripcariu A, Balan R, Avadanei ER and Căruntu ID: Heterogeneous periostin expression in different histological variants of papillary thyroid carcinoma. Biomed Res Int 2017: 8701386, 2017.
28. Bai Y, Kakudo K, Nakamura M, Ozaki T, Li Y, Liu Z, Mori I, Miyauchi A and Zhou G: Loss of cellular polarity/cohesiveness in the invasive front of papillary thyroid carcinoma and periostin expression. Cancer Lett 281: 188-195, 2009.
29. Bai Y, Nakamura M, Zhou G, Li Y, Liu Z, Ozaki T, Mori I and Kakudo K: Novel isoforms of periostin expressed in the human thyroid. Jpn Clin Med 1: 13-20, 2010.
30. Fluge Ø, Bruland O, Akslen LA, Lillehaug JR and Varhaug JE: Gene expression in poorly differentiated papillary thyroid carcinomas. Thyroid 16: 161-175, 2006.
31. Lee JW, Bae SH, Jeong JW, Kim SH and Kim KW: Hypoxia-inducible factor (HIF-1)alpha: Its protein stability and biological functions. Exp Mol Med 36: 1-12, 2004.
32. Maxwell PH, Wiesener MS, Chang GW, Clifford SC, Vaux EC, Cockman ME, Wykoff CC, Pugh CW, Maher ER and Ratcliffe PJ: The tumour suppressor protein VHL targets hypoxia-inducible factors for oxygen-dependent proteolysis. Nature 399: 271-275, 1999.
33. Ivan M, Kondo K, Yang H, Kim W, Valiando J, Ohh M, Salic A, Asara JM, Lane WS and Kaelin WG Jr: HIFalpha targeted for VHL-mediated destruction by proline hydroxylation: Implications for O$_2$ sensing. Science 292: 464-468, 2001.
34. Formenti F, Constantin-Teodosiu D, Emmanuel Y, Cheeseman J, Dorrington KL, Edwards LM, Humphreys SM, Lappin TR, McMullin MF, McNamara CJ, et al: Regulation of human metabolism by hypoxia-inducible factor. Proc Natl Acad Sci USA 107: 12722-12727, 2010.
35. Ruas JL, Poellinger L and Pereira T: Role of CBP in regulating HIF-1-mediated activation of transcription. J Cell Sci 118: 301-311, 2005.
36. Forsythe JA, Jiang BH, Iyer NV, Agani F, Leung SW, Koos RD and Semenza GL: Activation of vascular endothelial growth factor gene transcription by hypoxia-inducible factor 1. Mol Cell Biol 16: 4604-4613, 1996.
37. Kim JW, Tchernyshyov I, Semenza GL and Dang CV: HIF-1-mediated expression of pyruvate dehydrogenase kinase: A metabolic switch required for cellular adaptation to hypoxia. Cell Metab 3: 177-185, 2006.
38. Schmid T, Zhou J and Brüne B: HIF-1 and p53: Communication of transcription factors under hypoxia. J Cell Mol Med 8: 423-431, 2004.
39. Kudo A: Introductory review: Periostin-gene and protein structure. Cell Mol Life Sci 74: 4259-4268, 2017.
40. Srinivasan S, Guha M, Dong DW, Whelan KA, Ruthel G, Uchikado Y, Natsugoe S, Nakagawa H and Avadhani NG: Disruption of cytochrome c oxidase function induces the Warburg effect and metabolic reprogramming. Oncogene 35: 1585-1595, 2016.
41. Zhang Z, Nie F, Kang C, Chen B, Qin Z, Ma J, Ma Y and Zhao X: Increased periostin expression affects the proliferation, collagen synthesis, migration and invasion of keloid fibroblasts under hypoxic conditions. Int J Mol Med 34: 253-261, 2014.
42. Aukkarasongsup P, Haruyama N, Matsumoto T, Shiga M and Moriyama K: Periostin inhibits hypoxia-induced apoptosis in human periodontal ligament cells via TGF-β signaling. Biochem Biophys Res Commun 441: 126-132, 2013.
43. Guo X, Xue H, Shao Q, Wang J, Guo X, Chen X, Zhang J, Xu S, Li T, Zhang P, et al: Hypoxia promotes glioma-associated macrophage infiltration via periostin and subsequent M2 polarization by upregulating TGF-beta and M-CSFR. Oncotarget 7: 80521-80542, 2016.
44. Liu Y, Gao F and Song W: Periostin contributes to arsenic trioxide resistance in hepatocellular carcinoma cells under hypoxia. Biomed Pharmacother 88: 342-348, 2017.
45. Vaupel P and Multhoff G: Revisiting the Warburg effect: Historical dogma versus current understanding. J Physiol 599: 1745-1757, 2021.

46. Yang Z, Huang R, Wei X, Yu W, Min Z and Ye M: The SIRT6-autophagy-Warburg effect axis in papillary thyroid cancer. Front Oncol 10: 1265, 2020.
47. Semenza GL: Hypoxia-inducible factor 1: Regulator of mitochondrial metabolism and mediator of ischemic preconditioning. Biochim Biophys Acta 1813: 1263-1268, 2011.
48. Zhang H, Bosch-Marce M, Shimoda LA, Tan YS, Baek JH, Wesley JB, Gonzalez FJ and Semenza GL: Mitochondrial autophagy is an HIF-1-dependent adaptive metabolic response to hypoxia. J Biol Chem 283: 10892-10903, 2008.
49. Ordureau A, Münch C and Harper JW: Quantifying ubiquitin signaling. Mol Cell 58: 660-676, 2015.
50. Zhang W: The mitophagy receptor FUN14 domain-containing 1 (FUNDC1): A promising biomarker and potential therapeutic target of human diseases. Genes Dis 8: 640-654, 2020.
51. Zhang W, Ren H, Xu C, Zhu C, Wu H, Liu D, Wang J, Liu L, Li W, Ma Q, *et al*: Hypoxic mitophagy regulates mitochondrial quality and platelet activation and determines severity of I/R heart injury. Elife 5: e21407, 2016.